Optical Constants of Amorphous Zinc Arsenide (Zn_3As_2) via Spectroscopic Ellipsometry

James Colter Stewart

A senior thesis submitted to the faculty of

Brigham Young University

In partial fulfillment of the requirements for the degree of

Bachelor of Science

John Colton, Advisor

Department of Physics and Astronomy

Brigham Young University

April 2019

ABSTRACT

Optical Constants of Amorphous Zinc Arsenide (Zn_3As_2) via Spectroscopic Ellipsometry

James Colter Stewart

Department of Physics and Astronomy

Bachelor of Science

Zinc oxide (ZnO) is a promising wide band gap semiconductor with applications in ultraviolet optoelectronics. Through a novel sputtering process, our group seeks to create arsenic-doped p-type ZnO. In order to characterize these samples, we must understand the thin evaporated zinc arsenide (Zn_3As_2) layer in between the sputtered ZnO and our substrates. We characterize these samples by variable-angle spectroscopic ellipsometry (VASE), scanning electron microscopy (SEM), and X-ray diffraction (XRD). Enclosed is a paper our research group has submitted to Optics Express that reports the results of these characterizations; these results show that a five-parameter ellipsometric model is sufficient to find the optical constants for amorphous Zn_3As_2 samples. Further work needs to be done in order to properly characterize crystalline Zn_3As_2 samples via ellipsometry.

Keywords: ellipsometry; zinc oxide; zinc arsenide; scanning electron microscopy (SEM); X-ray diffraction (XRD)

Acknowledgments

I would first like to thank my mentors Drs. John Colton and David Allred for their guidance and support of this project. Dr. Allred spent more than one Saturday with me on campus helping with the writing of the paper that comprises the bulk of this thesis. I'd also like to thank my high school physics and chemistry teacher, Dennis Johnson, for introducing me to the subject of physics. My parents, Marsden and Leelee Stewart, deserve special thanks for their support of me in high school and their encouragement to go to college and study what I found most meaningful. And finally, the biggest thanks go to my darling wife, Makenna, for her unwavering support of me in all my scholarly and career pursuits.

Table of Contents

List of Figures

List of Tables

Chapter 1 Introduction

Motivation

Semiconductor devices are essential for electronic circuits, computers, and optical devices. Presently, gallium nitride (GaN) is used to produce many high-energy, high-temperature optical devices; however, zinc oxide (ZnO) has been recognized not only as a cheaper alternative to GaN but could also have superior physical and optical properties [i] (Please note that references in this thesis are different than those found in Chapter 2, which contains a paper our group is submitting for publication. For this reason, I have chosen to number references in this thesis with lower-case Roman numerals, while I use Arabic numerals for the references in the paper). Semiconductors are characterized primarily by a quantity called the band gap. The band gap of a material is a range of energy states where no electrons can exist. When electrons fall from a more energetic state above the band gap to a less energetic one below, a photon is released; thus, the band gap is a measure of how a material interacts with light. ZnO has several advantages over GaN: along with its wider band gap of 3.66 eV (compared to 3.4 eV for GaN), it can be fabricated uniformly on various substrates, whereas GaN is only produced on limited substrates, and the growth temperature for high-quality ZnO is much less than that needed for GaN (~500° C compared to ~1000° C). Additionally, ZnO has a higher radiation tolerance than GaN [ii]. Devices that could be produced with ZnO include LEDs, UV lasers, and thin-film transistors (TFTs), among others. However, to make a working semiconductor device, both p-type and n-type semiconductors are needed. Through a process called doping impurities are introduced into a semiconductor crystal, which mix with the semiconductor atoms to produce

either an excess of bonding electrons (resulting in an n-type semiconductor) or an excess need for bonding electrons. This "need" for an electron is referred to as a hole, and is a positive charge carrier, resulting in a p-type semiconductor. Naturally occurring defects in ZnO, such as vacancies in the crystal lattice of the material, cause it to be n-type; reliable, reproducible p-type ZnO has not yet been produced [iii]. This has become the biggest obstacle in the commercialization of zinc oxide [i].

Look et al. report that by sputtering a thin film of zinc oxide onto a heated zinc arsenide (Zn_3As_2)-coated substrate, the resulting films were heavily p-type doped [iv,v]. For a detailed description of this novel sputtering process, refer to Refs. 4 and 5, and to Ryan Peterson's 2018 senior thesis, submitted to this department [vi]. Once these films are made, it is necessary to find their thickness so their dopant concentrations can be measured. We determine their thickness with a technique called variable-angle spectroscopic ellipsometry (VASE). A description of ellipsometry is provided herein.

Our group quickly discovered that these thin-film ZnO samples were impossible to characterize via ellipsometry without understanding the optical properties and thickness of the Zn_3As_2 layer underneath it. This is the motivation for the work described in this thesis.

Description of Ellipsometry

For our ellipsometry measurements, we use a J.A. Woollam M2000 variable-angle spectroscopic ellipsometer. In order to analyze our ellipsometric data, we use a software suite made by the same company called WVASE. Ellipsometry is a non-invasive technique used to determine the thickness, roughness, uniformity, and complex refractive index of thin films. A graphic of a typical ellipsometer setup is shown in Figure 1.1.

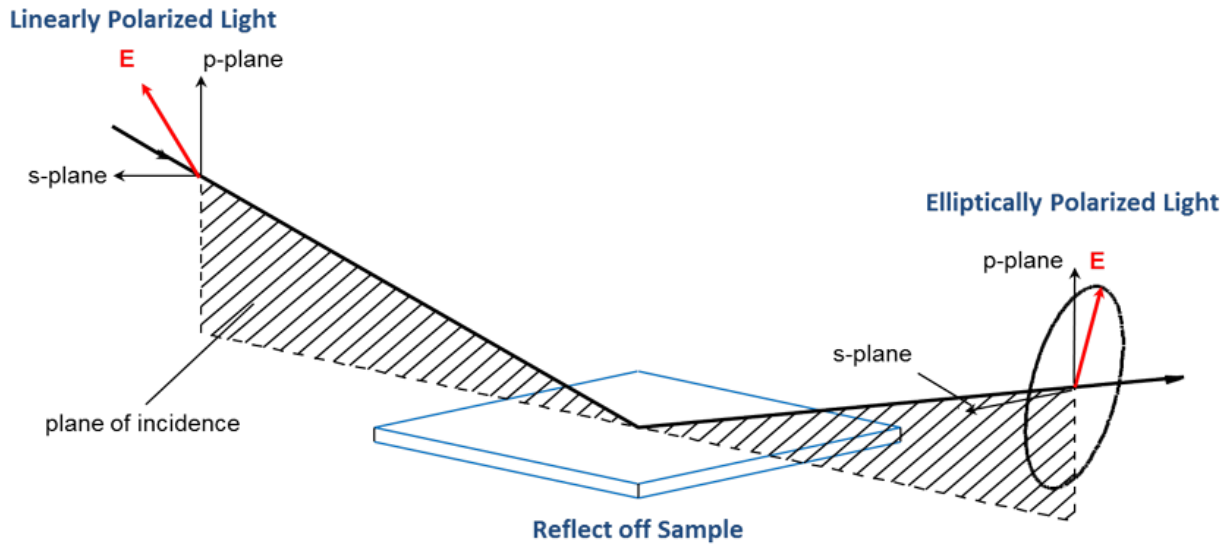

Figure 1.1. Ellipsometry setup. Light from the source is polarized linearly, and then reflects off of the sample surface. It is then analyzed, and the change in polarization is measured. Image from Ref. [vii].

In an ellipsometric measurement, the incident light is polarized linearly with components perpendicular to the direction of travel in two planes: the plane of incidence (see Fig. 1.1, also known as the p-plane or parallel plane) and the corresponding perpendicular plane (also called the s-plane). Polarization of light describes the direction in which the electric and magnetic fields oscillate. Unpolarized light contains EM fields that oscillate in every direction. In linearly polarized light, each field oscillates in only one direction; Figure 1.1 shows this as the red electric field vector in the upper-left corner of the figure (the magnetic field is perpendicular to that). This electric field vector only changes magnitude in time and does not change direction in the polarization plane. In other words, the components in the p-plane and s-plane are perfectly in phase with one another.

After reflecting off the sample surface, the light becomes elliptically polarized. Elliptically polarized light is characterized by an electric field vector where the p-plane components and s-plane components are out of phase with each other. In Figure 1.1, this is shown as the ellipse on the right-hand side of the figure; this is the path that the electric field

vector traces in time. If the p-plane and s-plane components are perfectly out of phase with each other and equal in amplitude, the light is circularly polarized, because the traced path of the electric field vector is a circle. To characterize the change to elliptical polarization, ellipsometry measures two parameters, Ψ and Δ, which are defined by the following equation:

$$\rho = \frac{r_p}{r_s} = \tan \Psi \, e^{i\Delta}$$

The parameter ρ is called the complex reflectance ratio. The parameters r_p and r_s are the reflection amplitude coefficients for p- and s-polarizations, respectively. The reflection amplitude coefficient for a particular plane is the ratio of amplitude of reflected light in that plane (measured by the amplitude of the electric field vector) to the amplitude of incident light in that plane. In addition to the amplitudes of these two polarizations changing, they are no longer in phase with each other after reflection. Thus, Ψ measures the change in amplitude and Δ measures the phase shift between the two polarizations. These ellipsometric measurements are taken at various angles of incident light; our samples are measured at 60-80° to the normal. A very detailed description of the interaction between the incident light, sample surface, and reflected light can be found in Appendix A of Ref. viii. We use ellipsometry to measure the thicknesses of our zinc arsenide thin films. As an added feature, we also obtain the optical constants of the material.

Crystallinity of Thin Film Materials

Thin films (or solids in general) may typically be classified as either crystalline, polycrystalline, or amorphous. In order to understand the properties of our thin Zn_3As_2 films, we must understand the type of material we are dealing with. Crystalline materials are classified by

their highly repeatable order of molecules in space; all molecules fit together in the same pattern. Polycrystalline materials are like crystalline materials in that the molecules fit together nicely, but in smaller groups. These small groups are typically oriented randomly with respect to one another. Amorphous materials have rigid structures but no well-defined pattern. At the microscopic level, ordering and placement of molecules is completely random.

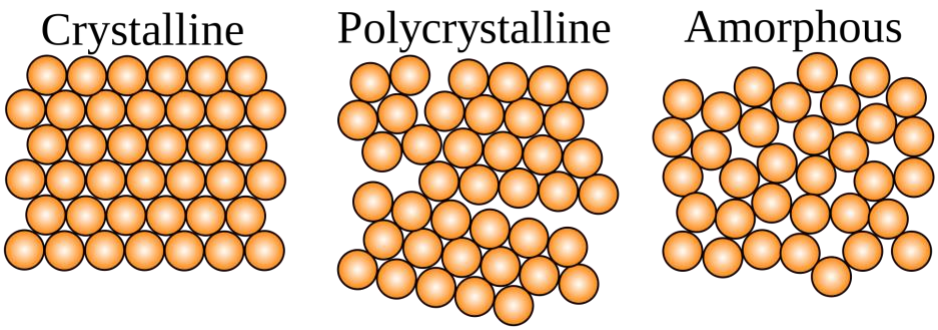

Figure 1.2. Structural differences in crystalline, polycrystalline, and amorphous materials. Image from Wikipedia [ix].

Figure 1.2 shows the differences between these three types of materials on a microscopic scale. The difference between structures gives rise to differences in how light interacts with a crystalline material vs. an amorphous material; this becomes important when we analyze our ellipsometric data. In order to characterize the structure of our zinc arsenide films, we employ both scanning electron microscopy (SEM) and X-ray diffraction (XRD). These two types of measurements were performed by my colleagues Daniel Boyce and Micah Shelley. Detailed descriptions of SEM and XRD are found in Refs. x and xi, respectively.

Overview

The primary goal of this thesis is to present and discuss the methods used for evaporating and characterizing our thin Zn_3As_2 films. This introduction has discussed the motivation for this

project, particularly its applications in the fabrication of p-ZnO. It has also provided a brief introduction to ellipsometry.

Chapter 2 contains a paper that our group has submitted for publication to Optics Express, a peer-reviewed journal published by The Optical Society (OSA). The primary authors of this paper are myself and Drs. David Allred and John Colton. Dr. Allred wrote the introduction, conclusion, and abstract for the paper. I made significant contributions to the "Experimental technique" section and the "Results and Discussion" section. Dr. Colton was instrumental in editing and providing feedback to prepare the paper for publication. Micah Shelley, Spencer King, Daniel Boyce, and Nathan Schwartz are fellow members of Dr. Colton's research group who helped take and analyze data that is presented in the paper. Please note that the formatting of Chapter 2 is different than the rest of this thesis; it was written for submission to Optics Express and is formatted as such.

Chapter 3 contains additional conclusions, outside of those made in our paper. Specifically, this chapter discusses how the results from our work on Zn_3As_2 can now help further our work with the fabrication of p-ZnO films.

Chapter 2 Paper for publication

Optical constants of evaporated amorphous zinc arsenide (Zn_3As_2) via spectroscopic ellipsometry

J. COLTER STEWART, MICAH N. SHELLEY, NATHAN R. SCHWARTZ, SPENCER K. KING, DANIEL W. BOYCE, DAVID D. ALLRED* AND JOHN S. COLTON

Department of Physics and Astronomy, Brigham Young University, Provo, UT 84602, USA
**dda@byu.edu*

Abstract: We have used spectroscopic ellipsometry to measure the optical constants of evaporated amorphous zinc arsenide (Zn_3As_2). A five parameter model using a Tauc-Lorentz oscillator was found to fit well each of six amorphous samples deposited on Si_3N_4/silicon, allowing the layer thicknesses and optical constants to be deduced. Layer thicknesses varied from 20 to 70 nm. The fitted value of the optical gap (Tauc gap) is 0.95 eV, close to the 1.0 eV band gap for crystalline bulk zinc arsenide. A single set of parameters from an ensemble Tauc-Lorentz model can be used to determine the thicknesses of amorphous Zn_3As_2 layers as long as the layers are $\gtrsim$ 25 nm thick. Measured film thicknesses do not correlate with targeted thicknesses, likely due to inconsistent nucleation times.

1. Introduction

Presently, gallium nitride (GaN) is used to produce many high-energy, high-temperature optical devices. However, zinc oxide (ZnO) has been recognized as a potentially cheaper alternative to GaN, possibly also with superior physical, electronic and optical properties [1]. A major obstacle in the optoelectronic commercialization of ZnO has proven to be naturally occurring defects such as lattice vacancies which cause nominally undoped material to be n-type, and compensate added p-type dopants. Reliable and reproducible heavily-doped p-type ZnO has not yet been commercialized [2]. Look et al. reported that good quality heavily p-type ZnO films could be produced by sputtering ZnO onto a hot zinc arsenide (Zn_3As_2)-coated substrate [3,4]. The Zn_3As_2 coating was achieved by evaporation. Several p-type doped ZnO samples were produced which maintained their electrical properties after a decade. Our interest in thin-film zinc arsenide therefore arises out of its use as a source for arsenic doping of zinc oxide in this novel evaporation/sputter process.

Our research presented here has found that evaporated Zn_3As_2 films are often amorphous, and in attempting to use spectroscopic ellipsometry to characterize the thickness of amorphous Zn_3As_2 films, we have found the published optical constants of Zn_3As_2 [5] to be inadequate. We have developed a Tauc-Lorentz oscillator model to fit our ellipsometric data which provides optical constants and allows thicknesses to be determined.

2. Experimental technique

Zinc arsenide samples are made by evaporating powdered Zn_3As_2 onto various substrates. Those samples are then characterized by scanning electron microscopy (SEM), X-ray diffraction (XRD), and variable-angle, spectroscopic ellipsometry (VASE).

2.1 Sample Preparation

Powdered Zn_3As_2 (Chemsavers ZNARSN100G, 99.9% grade) is placed in a tungsten boat (RD Mathis) in a Denton 502A Deposition System. The substrates are attached facing downward on a 10 cm diameter substrate holder using Kapton tape. This holder is located 23 cm above the boat and is attached to a chain-driven planetary system that rotates and rocks the holder in a quasi-nonrepeating pattern when energized. This evens out the deposited film thickness across the substrates. The chamber is closed and evacuated, typically to less than 2×10^{-6} torr and frequently to below 5×10^{-7} torr. Once the chamber has reached sufficiently low pressure, we begin to slowly ramp up the current, reaching approximately 120 amps in just over 1 min. At about 100 amps, a quartz crystal thin film deposition monitor (Inficon model XTM/2) indicates evaporation has commenced. This device monitors thickness by measuring the change in frequency of a quartz crystal resonator as a film is deposited. The substrate holder planetary, set at 50% of maximum rotation speed, is activated, setting the substrate holder into motion. Once the target deposition rate of greater than 0.2 nm/s is reached, the shutter between the source and the substrate is opened and deposition on the substrate commences. Multiple substrates can be evaporated onto simultaneously. The deposition rate invariably increases substantially as the evaporation continues, and after reaching the pre-programmed thickness on the quartz crystal monitor, the shutter automatically closes. The chamber is then vented with dry nitrogen, and the coated substrates are removed and promptly taken to have their thicknesses measured via spectroscopic ellipsometry.

2.2 Optical characterization

A J.A. Woollam M2000 variable-angle, spectroscopic ellipsometer is used to make measurements of thicknesses and optical constants. The usual substrates chosen for thickness determination are cleaved from 200 mm diameter, polished (100) Si test wafers coated with 300 nm (nominal thickness) CVD-grown silicon nitride (Si_3N_4) and are called "Si_3N_4/silicon" below. The rationale for using a layer of Si_3N_4 for thickness and optical constants measurements comes from Hilfiker et al.'s work on characterizing thin absorbing films with spectroscopic ellipsometry [6]. They observed that it was difficult to measure the optical constants and thicknesses of thin absorbing materials deposited directly onto a silicon substrate. Ellipsometric measurements made on absorbing layers on silicon do not yield as reliable of thicknesses and optical constants as they do for transparent layers. Hilfiker et al. found that if a thin transparent spacer layer is added between an absorbing layer with unknown optical constants and the silicon substrate, then the ellipsometric measurements produce unique information as they would for a transparent film. Thus, we chose the following configuration for characterizing evaporated zinc arsenide (from top to bottom): an unknown thickness of Zn_3As_2 (the partially absorbing layer), on 300 nm of Si_3N_4 (the transparent spacer layer), on a silicon substrate. To say that the Zn_3As_2 is *partially* absorbing means that over a portion of the energy range that the samples were studied, light could penetrate and reflect off the Zn_3As_2/Si_3N_4 interface. This range is the portion below the material's optical gap, which at room temperature is about 1.0 eV for bulk Zn_3As_2 [7]. In addition, as shown below, due to the thinness of the layers, the Zn_3As_2 samples we prepared remain partially transparent for about 1.5 eV above this.

Ellipsometry measures the reflectivity of p- and s-polarized light. A measurement for a given wavelength and a given angle of incident light can be summarized by two parameters, Ψ and Δ, for which the defining equation is:

$$\frac{r_p}{r_s} = \tan\Psi\, e^{i\Delta} \tag{1}$$

The parameters r_p and r_s are the reflection amplitude coefficients. Thus, the parameter Ψ describes the ratio of amplitudes of reflections from the two polarizations whereas the parameter Δ describes the change in phase of the reflections. Measurements are done as a function of wavelength at various incident angles. Specifically, in our case we have taken data with incident angles at 5° increments between 60-80° (all angles measured relative to the normal). That is, for every sample, for each of the five angles we obtain a set of measurements of the ellipsometric parameters, Ψ and Δ, taken as functions of wavelength.

The angles that we measured were chosen to encompass the Brewster's angles of both silicon and silicon nitride, which in the visible range are about 76˚ and 63˚, respectively [8]. Bulk Zn_3As_2 is also expected to have its Brewster's angle in this range, at about 77° [5]. For a bulk material with little or no absorption, r_p vanishes at Brewster's angle so the ellipsometric parameter Ψ becomes zero or very small. This makes measurements close to Brewster's angle particularly useful in determining the optical constants of materials [9]. Assuming the optical constants of materials are known or can otherwise be determined, fits of the ellipsometric data can then be done to determine layer thicknesses.

In addition to the Si_3N_4/silicon substrates, we have also evaporated Zn_3As_2 onto glass microscope slides and onto sapphire (Al_2O_3) substrates. The sapphire substrates were chosen due to their potential of creating single crystal ZnO films as the ZnO lattice aligns itself with the oxygen sublattice in Al_2O_3, despite an 18% lattice mismatch [10]. Studying the Zn_3As_2 films deposited on Si_3N_4/silicon and on glass was thus originally intended as a stepping stone to studying films on sapphire.

2.3 Structural measurements

In order to better understand the physical structure of our Zn_3As_2 thin films, we measure surfaces with a Verios G4 UC scanning electron microscope (SEM) and perform X-ray diffraction (XRD) with a PANalytical X'Pert Pro MPD X-ray diffractometer at the Cu K_α line. The XRD yields information about differences in crystallinity between samples, and the SEM gives structural information and provides a check on the roughness information obtained from ellipsometry.

3. Results and discussion

3.1 Structural

Zn_3As_2 films on sapphire and on Si_3N_4/silicon were examined by SEM. Figures 1(a) and (b) show representative micrographs of films grown on these two types of substrates, respectively. The magnification of each picture was adjusted so that the picture is 1 μm^2 area of the samples.

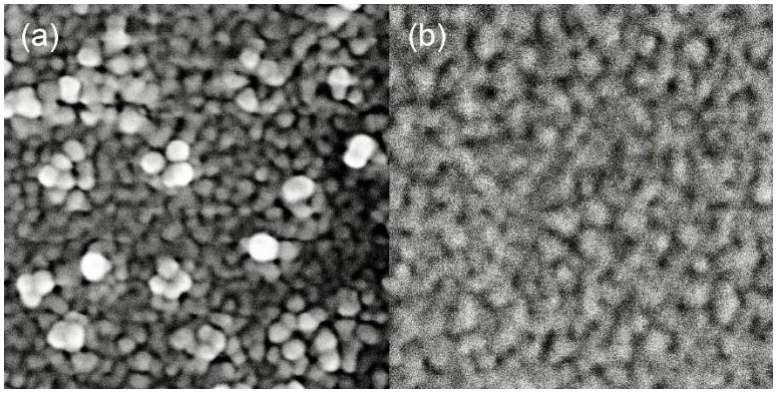

Figure 2.1. Representative SEM images of Zn_3As_2 samples on (a) sapphire and (b) Si_3N_4/silicon (right). Each image displays a 1 μm^2 area of the samples.

Fig. 2.1(a) shows the formation of polycrystalline Zn_3As_2 on a sapphire substrate, likely via an island-growth mechanism such as Volmer–Weber (VW) growth although the Stranski–Krastanov mechanism cannot be ruled out [11,12]. VW growth occurs when atoms or molecules in the evaporant are more strongly bound to each other than to substrate atoms, and is often seen in the growth of semiconductors on oxides [11] as is the case here.

As seen in Fig. 2.1(a), the Zn_3As_2 deposited on sapphire is composed mainly of many small, distinct masses, roughly 30-50 nm in size. Most are separated from some of their neighbors by voids or high-aspect-ratio cracks. This surface is noticeably rougher than the Zn_3As_2 grown on Si_3N_4/silicon, shown in Fig. 1(b). In addition, there are numerous grains whose top surfaces appear to lie above most others. These are larger and appear bright in the micrograph. This may be evidence of competitive growth with certain preferred crystallographic growth planes, which is common in thin-film growth. Several of the larger, isolated grains possess a hexagonal habit. In several spots, approximately equal-sized grains come together with angles of approximately 120° and are positioned relative to one another suggesting underlying symmetry templating their growth. This is suggestive of the (111) planes of a cubic crystal. Many smaller grains come together with 90° angles, while acute angles including 60° can also be seen. Previous investigators have noted that Zn_3As_2 had a rough surface when grown on a crystalline substrate; in their case this was done by metalorganic vapor-phase epitaxy (MOVPE) on InP [13].

On the other hand, the sample on Si_3N_4 shown in Fig. 2.1(b) is observed to have an "orange-peel" surface texture with curved surfaces, one feature flowing into another. (This was sample D, see Table 1 below.) Little evidence of crystallinity is seen. In fact, XRD spectra of samples on Si_3N_4/silicon and on glass substrates show they are amorphous; there are no peaks aside from those due to the (100) silicon substrate. That the films on Si_3N_4/silicon and on glass are amorphous is not too surprising; both glass and the Si_3N_4 layer on silicon are themselves amorphous. Moreover, arsenic is a glass-forming element in chalcogenide glasses. For example, arsenic trisulfide (As_2S_3) is usually amorphous as prepared [14]. By contrast, XRD spectra from samples on sapphire show multiple large peaks in addition to those due to the sapphire substrate, evidence that the material is polycrystalline. There is also evidence of preferred orientation of the Zn_3As_2 layers on sapphire, which is discussed more fully elsewhere [15].

3.2 Spectroscopic ellipsometry

In Fig. 2.2 we show representative ellipsometric data: Ψ and Δ measured at 70° for a sample grown on Si_3N_4/silicon. (This was sample E, see Table 1 below.) The solid blue line is the measured data for Ψ and the solid red line is the measured data for Δ. Model-generated data as explained below is overlaid on each plot with dashed lines. The example shown was deliberately chosen to not be an optimum fit, in order to more clearly show the differences between experimental and model-generated values. The curves in Fig. 2.2 are marked by oscillations at energies below about 2.5 eV (above 450 nm), while above 2.5 eV (below 450 nm) Ψ gradually increases. The position of the oscillations is determined primarily by the thickness of the 300 nm Si_3N_4 layer, while their amplitude and width are determined primarily by the absorption of the zinc arsenide layer. The ellipsometric spectrum of an uncoated silicon nitride sample shows narrower peaks with higher contrast [16].

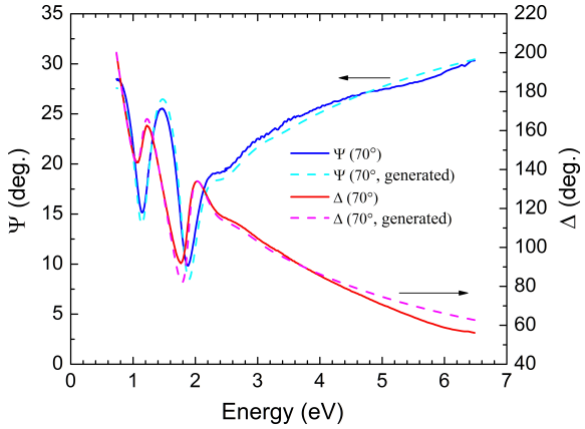

Figure 2.2. Representative Ψ and Δ values as a function of photon energy, E, measured at 70˚ for a sample of Zn_3As_2 on Si_3N_4/silicon. The solid lines represent experimental data. The model-generated data is overlaid on each plot with dashed lines.

Optical constants for bulk, crystalline Zn_3As_2 are available from *Handbook of Optical Constants of Solids*, *III*, and references cited therein [5]. These literature values were obtained by bulk reflectivity measurements, after which Kramers-Kronig (K-K) analysis was employed to obtain the optical constants. We first attempted to fit our ellipsometric data using these optical constants from the literature; however, this was unsuccessful. Therefore, as is standard for VASE, we modeled the optical constants of our films using a suite of oscillators. We selected various oscillators from J.A. Woollam's variable-angle spectroscopic ellipsometry software (WVASE) to build trial models. The aim with these trial models is to find a common set of parameters, called an ensemble model, that can be used to specify the optical constants of all of the evaporated films to facilitate thickness measurements. This is done by first fitting a model for each sample individually, and then allowing the model to adjust its parameters while fitting multiple samples simultaneously.

We found that the ellipsometric data of Zn_3As_2 on Si_3N_4/silicon for any individual sample could be well modeled, for the purpose of measuring thicknesses, with Woollam's general oscillator approach. The model consisted of three layers on a silicon substrate, namely (from bottom to top) a silicon substrate, a Si_3N_4 layer, a Zn_3As_2 layer, and finally a layer of Zn_3As_2 roughness. Roughness is defined as 50% underlayer material mixed with 50% void. The optical constants of the Si_3N_4 had previously been determined and were not allowed to vary. However, the Si_3N_4 thickness for a given sample was not precisely known and therefore was allowed to vary from 302 to 310 nm. For the Zn_3As_2 layers we found that a five parameter model could fit the data for each sample individually: a four parameter Tauc-Lorentz (TL) oscillator along with the value of ε_1 (the real part of the complex relative permittivity) at $E = \infty$.

The Tauc-Lorentz oscillator model is particularly well suited for amorphous materials. Tauc et al. proposed a model for understanding the optical gap of disordered materials by considering the general form of the joint density of states (JDOS) near the optical gap of disordered materials [17,18]. The optical gap for amorphous materials, also called the Tauc gap, is similar to crystalline materials' band gap. This description is adequate to describe the interaction of light near the band edges but is not K-K consistent. Jellison et al. derived a parametric model of the dielectric function of semiconductor and dielectric materials which added Lorentz (classical) oscillator broadening to Tauc's optical-gap approach, to obtain an optical JDOS [19]. With additional approximations concerning momentum transfer, etc., the TL model is generated [19,20].

The Tauc-Lorentz oscillator model calculates the relative permittivity function $\varepsilon = \varepsilon_1 + i\varepsilon_2$ of a material, where:

$$\varepsilon_2 = \begin{cases} \dfrac{A\,E_0\,C\left(E - E_g\right)^2}{\left(E^2 - {E_0}^2\right)^2 + C^2E^2} \cdot \dfrac{1}{E}, & E > E_g \\ 0, & E \le E_g \end{cases} \tag{2a}$$

$$\varepsilon_1 = \frac{2}{\pi} P \int_{E_g}^{\infty} \frac{\xi \varepsilon_2(\xi)}{\xi^2 - E^2} d\xi + \varepsilon_1(\infty) \tag{2b}$$

Here, ε_2 represents an absorption peak described by four parameters: A represents the amplitude of the peak, E_0 is the energy at which the peak reaches its maximum, E_g is the optical gap, and C is a measure of the peak width. The equation for ε_1 comes from the K-K transform of ε_2, with the fifth fitting parameter $\varepsilon_1(\infty)$ explicitly added in. The real and imaginary optical constants n and k can be calculated in the usual way from ε_1 and ε_2 (and vice versa) using the formulas

$$n + ik = \sqrt{\varepsilon_1 + i\varepsilon_2}, \tag{3a}$$

$$\varepsilon_1 = n^2 - k^2, \text{ and} \tag{3b}$$

$$\varepsilon_2 = 2nk. \tag{3c}$$

Since there are approximately 700 values of Ψ and Δ per measurement angle, this is a vastly overdetermined system.

The Cody-Lorentz (CL) oscillator model was also examined. This oscillator, like the Tauc-Lorentz oscillator, is designed specifically for amorphous semiconductors [20–22]. Though the model incorporates more adjustable parameters than the TL model, the fits obtained were not significantly different than those from the TL model, nor was the mean-squared error (MSE) of the CL fits any better. Thus, we judged the Tauc-Lorentz oscillator to be sufficient for our purposes.

For each sample, the thickness and roughness of the zinc arsenide, the five TL model parameters, and the Si_3N_4 thickness were allowed to vary. The results of the fits not only yield the Zn_3As_2 layer thicknesses and roughnesses, but also (through Eqs. 2 and 3) the optical constants of zinc arsenide. Sample-specific fits generally result in an MSE of less than 10. The MSE is an average of the squared difference between the model-generated data and the experimental data, weighted by the inverse error bar squared for each data point (so noisy points are weighted less heavily).

Table 1 shows the fitted thickness and roughness values for six samples of Zn_3As_2 on Si_3N_4/silicon, labeled samples A-F. The "Thickness Monitor Programmed Thickness" column indicates the targeted thickness via the Inficon quartz crystal monitor whereas the "Ellipsometry thickness" column is the value from the TL fits. The right three columns contain values obtained by fitting each sample to the ensemble model, discussed in more detail below.

Table 1. Thicknesses (nm) and Roughnesses (nm) of Zn_3As_2 layers on Si_3N_4/silicon.

Sample	Thickness Monitor Programmed Thickness	Individual Model Fits			Ensemble Model Fit		
		Ellipsometry Thickness	Roughness	MSE	Ellipsometry Thickness	Roughness	MSE
A	200	21.6	7.6	8.8	16.2	9.0	63.9
B	230	51.6	7.2	7.8	52.0	7.2	35.5
C	100	30.6	8.9	9.6	28.5	11.4	61.5
D	250	36.2	12.3	8.3	33.8	12.8	27.5
E	244	71.3	11.8	7.1	72.7	12.4	51.4
F	50	23.8	10.1	16.3	19.8	11.5	53.8
	Average		9.7	9.6		10.7	48.9
	Standard Deviation		2.0	3.1		2.0	3.1

The samples are all quite rough. The average roughness given by ellipsometry is fairly consistently about 10 nm, independent of thickness. Thus for the thinnest samples, the roughness comprises a significant fraction of the overall layer thickness. These values of the roughness are not inconsistent with SEM results.

3.3 Growth nucleation

There is perhaps surprisingly no correlation in Table 1 between a given sample's thickness according to the quartz crystal monitor and its thickness determined by ellipsometry. In no case was the film as thick as the monitor indicated. In addition, the ratio between the two thicknesses varied considerably. Even with the same target thickness set on the quartz crystal monitor, two independent evaporations could come out with vastly different thicknesses of Zn_3As_2. Moreover, some of our samples (not shown in the table) emerged with no detectible Zn_3As_2 on them at all.

This lack of correlation between targeted and measured thicknesses likely has do with the nucleation of growth on the substrate surface. As explained in the capillary model of thin film nucleation and growth, in the initial stages of deposition many atoms which strike a surface before nucleation has occurred will reevaporate from the surface [11]. Within this model, Zn_3As_2 films will only appear on the substrates after stable nucleation sites have appeared. If a collection of zinc arsenide molecules stick together on the substrate, a film forms that grows outward and thicker, but if an atom or molecule never finds a site to stick to other atoms, then the atoms eventually reevaporate and the sample comes out clean of any films.

To investigate this as a possible phenomenon, we placed a small video camera and light source in the evaporation chamber to record the growth of layers on the substrates. (For these videos, substrate rotation via planetary was not used.) We discovered that after the shutter is opened, many seconds elapse before the substrate shows the presence of any Zn_3As_2 layer growth; the presence of a Zn_3As_2 layer could be judged by a darkening of the substrate. As indicated by this darkening, the zinc arsenide film appears first at a single spot on the surface and then spreads outwards. The amount of time prior to darkening is highly variable, and significantly, the darkening of two different substrates placed side-by-side begins at different times and proceeds at different rates. Figure 2.3 shows a still frame from one of these evaporation videos; in it we see that the substrate on the left, a glass slide, has begun to darken before the right-hand sapphire substrate. This provides evidence that surface nucleation during evaporation occurs at random times after the shutter is opened, and explains the differences between targeted and measured film thicknesses. Specific nucleation sites could also often be identified in these videos by the outward spread of the darkening; what is unusual here is that

the nucleation—an atomic scale event—occurs only in one small area over a macroscopically large (many cm^2) area surface.

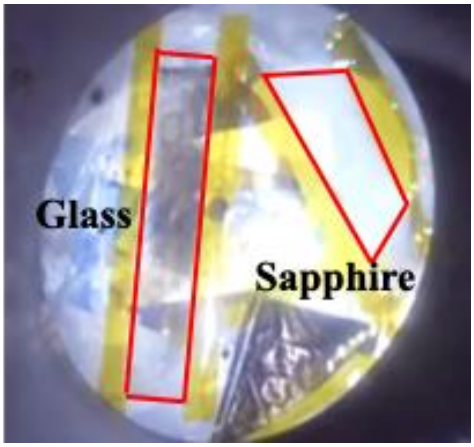

Figure 2.3. Still photo extracted from growth video during evaporation. The dark gray indicating Zn_3As_2 film growth develops on the left-hand substrate (glass) before it does on the right-hand substrate (sapphire). The amount of time from start of evaporation to darkening is highly variable from sample to sample.

3.4 Ensemble ellipsometric fits

Each sample listed in Table 1 required slightly different parameters for best fitting with the TL model. It is well known that the optical properties of many amorphous semiconductors vary from sample to sample, which is evidence that, in contrast with crystalline materials, there is not a single best "amorphous state" [23]. Thus, it is not particularly surprising that the fit parameters, and hence the optical constants, of the amorphous Zn_3As_2 layers on Si_3N_4/silicon vary from sample to sample. However, it is possible that these variations could result from a dependence of the optical constants on layer thickness. Therefore, it was desirable to see if parameters for an "average" TL model could be extracted that could adequately model the ellipsometric data from all samples A-F, regardless of thickness.

To accomplish this, we fitted the ellipsometric data from all six samples together in an ensemble model where the TL model's five parameters were not allowed to vary from sample to sample. (By contrast, the Zn_3As_2 thicknesses and roughnesses as well as the Si_3N_4 thicknesses were still allowed to be sample dependent.) This approach is termed multisample analysis, and can reduce parameter-parameter and parameter-thickness correlation effects, as well as increase parameter accuracy if the optical constants of the thin films are not thickness dependent [24]. We display the value of the parameters generated by this approach in Table 2.

Table 2. TL model parameter values from an ensemble fit of the six amorphous Zn_3As_2 on Si_3N_4/silicon samples.

Parameter	Value
A	129.0 ± 0.6
E_0	3.167 ± 0.004
E_g	0.952 ± 0.002
C	4.01 ± 0.01
$\varepsilon_1(\infty)$	1.52 ± 0.02

The layer thicknesses, roughnesses, and MSEs for samples A-F from the ensemble fit are displayed in Table 1 and can be compared to those values from the individual fits. The ensemble model caused the MSE to increase from an average of 9.6 to an average of 48.9. This increase in MSE is sufficiently large to negate the hypothesis that the material in all six samples is the same. However, as to the question of whether the optical constants obtained by the ensemble approach can be used to find the thicknesses of the films, the answer is generally yes. For the thickest films, there is a very good agreement between the thicknesses obtained through individual fits vs. the ensemble fit. The roughnesses also have generally good agreement. For the purpose of comparing the two types of fits, we compute an effective thickness as the sum of the thickness plus half of the roughness. The difference in effective thicknesses for samples B, C, D, and E is 5% or less. For samples A and F (the thinnest samples) it is 19% and 11%, respectively. Thus, we conclude that unless the layers are particularly thin ($\lesssim$ 25 nm), the amorphous Zn_3As_2 layer thicknesses can be well estimated by using the ensemble TL model fit parameters given in Table 2.

The fit parameters from Table 2 can therefore be used in Eqs. 2 and 3 to compute the optical constants of an "average" amorphous Zn_3As_2 layer. These optical constants, *n* and *k*, are plotted in Fig. 2.4, along with literature values for crystalline bulk Zn_3As_2 from Ref. [5]. The smoothness of our curve compared to the literature curve is to be expected since our optical constants come from an oscillator model which is only capable of generating smooth functions. Note, however, that our smooth functions do a much better job in the ellipsometry fits of the amorphous samples than do the literature values, and they depart from the literature values in significant ways. We provide tabulated values of our *n* and *k* functions in Appendix A. We also note that the ellipsometry data was only taken at energies from 0.7 to 6.5 eV; values presented in Fig. 4 and Appendix A for energies outside that range should be considered an extrapolation.

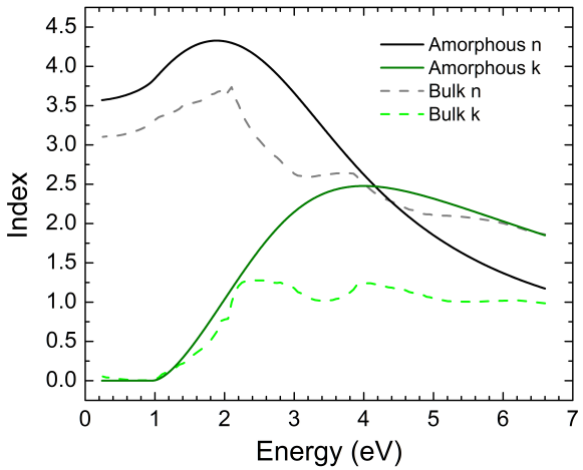

Figure 2.4. Optical constants (*n* and *k*) for our ensemble fit of six amorphous samples of Zn_3As_2 on Si_3N_4/silicon, compared to values for crystalline bulk Zn_3As_2 from Ref. [5].

E_g in Table 2 is the optical gap for our average amorphous Zn_3As_2 layer as determined by our ensemble fit. We note that it is close to the value of 1.0 eV for the room temperature band gap of crystalline Zn_2As_3 [7].

To test whether our ensemble model works well for amorphous Zn_3As_2 layers in general, we tested it with several samples of amorphous Zn_3As_2 grown on glass. Using the ensemble model *n* and *k* values and leaving only the Zn_3As_2 layer thickness and roughness as adjustable parameters, we were able to fit ellipsometric data for amorphous Zn_3As_2 layers on glass with MSE values similar to the ensemble model MSE values found in Table 1. Allowing the TL model parameters to vary for individual sample fits yielded MSE values similar to the

individual fit MSE values in Table 1. By contrast, attempts to use our ensemble model with Zn_3As_2 layers on sapphire failed; the MSE increased substantially. As discussed above, these are polycrystalline samples and are therefore expected to have different optical constants; the morphology of these samples also give rise to roughnesses comparable to the thicknesses of the films, which adds to the difficulty.

4. Summary and conclusions

Evaporated Zn_3As_2 layers deposited on Si_3N_4/silicon and on glass were determined to be amorphous by XRD and SEM, whereas Zn_3As_2 layers on sapphire are polycrystalline. Film thicknesses do not correlate with quartz crystal monitor values, likely due to nucleation of film growth occurring at random times after evaporation has begun.

Six samples grown on Si_3N_4/silicon were examined in detail by ellipsometry. Their roughness is about 10 nm, independent of thickness. The optical constants for all of these are well described by a Tauc-Lorentz model of the Zn_3As_2, with slightly varying parameters for their individual fits. A single set of parameters from the TL model and the optical constants derived from those parameters can be used to describe an "average" amorphous sample, and to determine the thicknesses of amorphous Zn_3As_2 layers as long as the layers are $\gtrsim 25$ nm thick. The optical gap given by the ensemble model is 0.95 eV, close to the 1.0 eV value for bulk zinc arsenide. The parameters/optical constants from the ensemble model also act as a good starting point for fitting samples using individual TL models. The TL model, however, does not work well for Zn_3As_2 grown on sapphire, likely due to the polycrystalline and rough nature of those films.

Funding

JCS, MNS, NRS, SKK, and DWB were supported by student grants by Brigham Young University's College of Physical and Mathematical Sciences.

Acknowledgments

We thank John E. Ellsworth for assistance with the Denton vacuum system, Stacy Smith for assistance in making XRD measurements and Prof. Matthew Linford and his students for assistance and guidance in using the M2000 spectroscopic ellipsometer.

References

1. Ü. Ozgur, D. Hofstetter, and H. Morkoç, "ZnO devices and applications: A review of current status and future prospects," Proc. IEEE **98**, 1255–1268 (2010).
2. D. C. Look, B. Claflin, Y. I. Alivov, and S. J. Park, "The future of ZnO light emitters," Phys. Status Solidi C Conf. **1**, 2203–2212 (2004).
3. D. C. Look, G. M. Renlund, R. H. Burgener, and J. R. Sizelove, "As-doped p-type ZnO produced by an evaporation/sputtering process," Appl. Phys. Lett. **85**, 5269–5271 (2004).
4. R. H. Burgener, R. L. Felix, and G. M. Renlund, "Fabrication of P-type Group II-VI Semiconductors," U.S. patent US 7141489 B2 (2006).
5. J. Misiewicz and K. Jezierski, "Zinc Arsenide (Zn3As2)," in *Handbook of Optical Constants of Solids, III*, E. D. Palik, ed. (Academic Press, 1998), pp. 595–607.
6. J. N. Hilfiker, N. Singh, T. Tiwald, D. Convey, S. M. Smith, J. H. Baker, and H. G. Tompkins, "Survey of methods to characterize thin absorbing films with Spectroscopic Ellipsometry," Thin Solid Films **516**, 7979–7989 (2008).
7. J. Misiewicz and J. M. Pawlikowski, "Optical band-gap of Zn3As2," Solid State Commun. **32**, 687–690 (1979).
8. D. E. Aspnes and A. A. Studna, "Dielectric functions and optical parameters of Si, Ge, GaP, GaAs, GaSb, InP, InAs, and InSb from 1.5 to 6.0 eV," Phys. Rev. B **27**, 985–1009 (1983).
9. M. Schubert, "Theory and Application of Generalized Ellipsometry," in *Handbook of Ellipsometry*, H. G. Tompkins and E. A. Irene, eds. (Springer, 2005), pp. 691–692.
10. Y. Chen, D. M. Bagnall, H. J. Koh, K. T. Park, K. Hiraga, Z. Zhu, and T. Yao, "Plasma assisted molecular beam epitaxy of ZnO on c-plane sapphire: Growth and characterization," J. Appl. Phys. **84**, 3912–3918 (1998).
11. M. Ohring, "Substrate Surfaces and Thin-Film Nucleation," in *Materials Science of Thin Films: Deposition and Structure*, 2nd ed. (Academic Press, 2002), pp. 357–415.
12. I. N. Stranski and L. Krastanow, "Zur Theorie der orientierten Ausscheidung von Ionenkristallen aufeinander,"

Monatshefte für Chemie und verwandte Teile anderer Wissenschaften **71**, 351–364 (1937).
13. D. J. Brink and J. A. A. Engelbrecht, "Ellipsometric investigation of rough zinc arsenide epilayers," Appl. Opt. **41**, 1894 (2007).
14. F. W. Glaze, D. H. Blackburn, J. S. Osmalov, D. Hubbard, and M. H. Black, "Properties of arsenic sulfide glass," J. Res. Natl. Bur. Stand. (1934). **59**, 83 (2012).
15. M. N. Shelley, S. K. King, B. J. Campbell, and J. S. Colton, "On the structure of bulk and thin film Zn3As2 (in preparation)," (n.d.).
16. D. D. Allred, R. S. Turley, S. M. Thomas, S. G. Willett, M. J. Greenburg, and S. B. Perry, "Adding EUV reflectance to aluminum-coated mirrors for space-based observation," Proc. SPIE - Int. Soc. Opt. Eng. **10398**, (2017).
17. J. Tauc, "Optical Properties of Amorphous Semiconductors and Solar Cells," in *Fundamentals of Semiconductors: Physics and Materials Properties*, P. Y. Yu and M. Cardona, eds. (Springer, 2012), pp. 566–568.
18. J. Tauc, R. Grigorovici, and A. Vancu, "Optical Properties and Electronic Structure of Amorphous Germanium," Phys. status solidi **15**, 627–637 (1966).
19. G. E. Jellison and F. A. Modine, "Parameterization of the optical functions of amorphous materials in the interband region," Appl. Phys. Lett. **69**, 371–373 (1996).
20. J. Orava, T. Wágner, J. Šik, J. Přikryl, M. Frumar, and L. Beneš, "Optical properties and phase change transition in Ge2 Sb2 Te5 flash evaporated thin films studied by temperature dependent spectroscopic ellipsometry," J. Appl. Phys. **104**, (2008).
21. G. D. Cody, "The Optical Absorption Edge of a-Si: H," in *Semiconductors and Semimetals, Vol. 21, Hydrogenated Amorphous Silicon, Part B, Optical Properties* (Academic Press, 1984), pp. 11–82.
22. J. Price, P. Y. Hung, T. Rhoad, B. Foran, and A. C. Diebold, "Spectroscopic ellipsometry characterization of HfxSiyOz films using the Cody–Lorentz parameterized model," Appl. Phys. Lett. **85**, 1701–1703 (2004).
23. M. Janai, D. D. Allred, D. C. Booth, and B. O. Seraphin, "Optical properties and structure of amorphous silicon films prepared by CVD," Sol. Energy Mater. **1**, 11–27 (1979).
24. W. A. McGahan, B. Johs, and J. A. Woollam, "Techniques for ellipsometric measurement of the thickness and optical constants of thin absorbing films," Thin Solid Films **234**, 443–446 (1993).

Chapter 3 Conclusion & Future Work

This chapter covers further conclusions than those presented in the paper in Chapter 2. The main focus is on future applications to our ZnO work.

As shown in Chapter 2, our work in finding the optical constants of Zn_3As_2 has been successful in the case of amorphous material. We have sputtered some samples of ZnO onto Zn_3As_2 on Si_3N_4 on Si; because we now have the optical constants for the zinc arsenide layer, it should be possible to find, within a small margin of error, the thickness of these ZnO samples. Once we know the thickness, we can reliably measure their carrier (dopant) concentrations.

We still have trouble fitting zinc arsenide grown on sapphire substrates, which are crystalline. Because of this, it is still difficult for us to characterize ZnO samples grown on sapphire. This is especially troubling because the previously made samples of p-ZnO were typically grown on sapphire substrates precisely because the substrate is crystalline; with a crystalline substrate, we expect that the ZnO layer is also crystalline [vi]. This doesn't mean that we cannot characterize these samples eventually; we simply need a different ellipsometric model. Recall that the Tauc-Lorentz oscillator used in our model is made specifically for characterizing *amorphous* semiconductors. Because of this, it is not surprising that our model only works for these types of layers. Theoretically, we should be able to develop a different oscillator model that can fit well those layers grown on crystalline substrates.

Appendix A: Tabulated *n* & *k* values

Tabulated values of the *n* and *k* optical constants for the ensemble Tauc-Lorentz oscillator model of amorphous zinc arsenide (Zn_3As_2), as shown in Fig. 2.4 and as calculated by the Table 2 parameters via Eqs. 2 and 3, found in Chapter 2.

eV	nm	*n*	*k*
0.25	4959.0	3.571	0.000
0.30	4133.0	3.577	0.000
0.35	3542.0	3.584	0.000
0.40	3100.0	3.592	0.000
0.45	2755.0	3.601	0.000
0.50	2480.0	3.612	0.000
0.55	2254.0	3.624	0.000
0.60	2066.0	3.638	0.000
0.65	1907.0	3.653	0.000
0.70	1771.0	3.671	0.000
0.75	1653.0	3.690	0.000
0.80	1550.0	3.712	0.000
0.85	1459.0	3.737	0.000
0.90	1378.0	3.766	0.000
0.95	1305.0	3.801	0.000
1.00	1240.0	3.845	0.005
1.05	1181.0	3.892	0.020
1.10	1127.0	3.940	0.043
1.15	1078.0	3.986	0.072
1.20	1033.0	4.030	0.108
1.25	991.9	4.071	0.148
1.30	953.7	4.110	0.192
1.35	918.4	4.145	0.240
1.40	885.6	4.177	0.291
1.45	855.1	4.207	0.345
1.50	826.6	4.233	0.401
1.55	799.9	4.256	0.459
1.60	774.9	4.275	0.519
1.65	751.4	4.292	0.580
1.70	729.3	4.305	0.643
1.75	708.5	4.315	0.707
1.80	688.8	4.322	0.771

eV	nm	*n*	*k*
1.85	670.2	4.326	0.837
1.90	652.5	4.327	0.903
1.95	635.8	4.325	0.969
2.00	619.9	4.319	1.035
2.05	604.8	4.310	1.101
2.10	590.4	4.299	1.167
2.15	576.7	4.284	1.233
2.20	563.6	4.267	1.298
2.25	551.0	4.246	1.362
2.30	539.1	4.223	1.426
2.35	527.6	4.197	1.488
2.40	516.6	4.168	1.550
2.45	506.1	4.137	1.609
2.50	495.9	4.103	1.668
2.55	486.2	4.067	1.725
2.60	476.9	4.029	1.780
2.65	467.9	3.989	1.833
2.70	459.2	3.947	1.884
2.75	450.9	3.903	1.933
2.80	442.8	3.857	1.980
2.85	435.0	3.810	2.025
2.90	427.5	3.762	2.068
2.95	420.3	3.712	2.109
3.00	413.3	3.661	2.147
3.05	406.5	3.610	2.183
3.10	399.9	3.558	2.216
3.15	393.6	3.505	2.248
3.20	387.5	3.451	2.277
3.25	381.5	3.398	2.304
3.30	375.7	3.344	2.328
3.35	370.1	3.290	2.351
3.40	364.7	3.236	2.371

eV	nm	*n*	*k*
3.45	359.4	3.182	2.390
3.50	354.2	3.129	2.406
3.55	349.3	3.076	2.421
3.60	344.4	3.023	2.434
3.65	339.7	2.971	2.445
3.70	335.1	2.919	2.454
3.75	330.6	2.868	2.461
3.80	326.3	2.817	2.468
3.85	322.0	2.767	2.472
3.90	317.9	2.718	2.475
3.95	313.9	2.670	2.477
4.00	310.0	2.623	2.478
4.05	306.1	2.576	2.477
4.10	302.4	2.530	2.476
4.15	298.8	2.485	2.473
4.20	295.2	2.441	2.469
4.25	291.7	2.398	2.464
4.30	288.3	2.355	2.459
4.35	285.0	2.314	2.452
4.40	281.8	2.273	2.445
4.45	278.6	2.233	2.438
4.50	275.5	2.194	2.429
4.55	272.5	2.156	2.420
4.60	269.5	2.119	2.410
4.65	266.6	2.083	2.400
4.70	263.8	2.048	2.389
4.75	261.0	2.013	2.378
4.80	258.3	1.979	2.367
4.85	255.6	1.946	2.355
4.90	253.0	1.914	2.342
4.95	250.5	1.882	2.330
5.00	248.0	1.851	2.317

eV	nm	*n*	*k*
5.05	245.5	1.821	2.304
5.10	243.1	1.792	2.290
5.15	240.7	1.763	2.277
5.20	238.4	1.735	2.263
5.25	236.2	1.708	2.249
5.30	233.9	1.682	2.235
5.35	231.7	1.656	2.220
5.40	229.6	1.630	2.206
5.45	227.5	1.606	2.191
5.50	225.4	1.581	2.177
5.55	223.4	1.558	2.162
5.60	221.4	1.535	2.147
5.65	219.4	1.512	2.132
5.70	217.5	1.490	2.117
5.75	215.6	1.469	2.102
5.80	213.8	1.448	2.088
5.85	211.9	1.428	2.073
5.90	210.1	1.408	2.058
5.95	208.4	1.388	2.043
6.00	206.6	1.369	2.028
6.05	204.9	1.351	2.013
6.10	203.3	1.333	1.998
6.15	201.6	1.315	1.983
6.20	200.0	1.298	1.968
6.25	198.4	1.281	1.953
6.30	196.8	1.264	1.938
6.35	195.3	1.248	1.924
6.40	193.7	1.232	1.909
6.45	192.2	1.217	1.894
6.50	190.7	1.202	1.880
6.55	189.3	1.187	1.865
6.60	187.9	1.173	1.851

Appendix B: Operating the Denton 502A Deposition System

This appendix contains the standard operating procedure for the evaporation system used for our samples (Denton 502A, located in room U-234 ESC).

NOTE: many of the switches are toggle switches. Pushing them will turn them on if they are off, and off if they are on. To turn on a switch, push the button, to turn it off push it again.

1. Find the control panel on the front of the instrument.
2. Turn on the system by pressing the black ON SYSTEM switch at the lower left corner of the control panel. It is a rocker switch.
3. Turn on the mechanical pump. That is, the switched labelled "MECH PUMP". It is a white rocker switch to the right of the System ON switch.
4. Turn the PRESSURE GAUGE SELECTOR to foreline. It is to the right of the Mech. Pump Switch by about 16 in.
5. When the foreline pressure drops below 50 mTorr (usually a few seconds), open the BACKING VALVE. It is a toggle switch above the black switches. Note that all the switches on that row light up when they are on.
6. When the press drops below 50 mTorr again, turn on the HI-VAC PUMP POWER SWITCH. It is in the same row as the black rocker switches. It is not the High vacuum gate valve switch on the row above. You should make sure that the gate valve is closed. It will be unlit.
7. Note the time you did this in your lab book. This is so that you will know how long the high vacuum pump has been on. The high vacuum pump is a diffusion

pump. You should read about diffusion pumps if you are not familiar with them. They must be "backed" when they are hot. Backing means that the mechanical pump is actively removing gas that they diffusion pump has compressed They will not pump until the diffusion pump oil inside them is hot. This usually takes 10 to 15 minutes.

The system should have been left under vacuum. In this case you must vent it.

8. Make sure that the ROUGHING VALVE is closed. Vent the chamber by turning on the N_2 tank on the south wall, and open the line going to the Denton evaporator. The pressure on the regulator should not be over about 10 psi (gauge). If it is over this amount the Bell jar will "pop up" when it reached the atmospheric pressure. This is not good.
9. Then open the VENT VALVE by pressing the 4^{th} toggle switch from the left on the top row of switches. It will light up.
10. After a few minutes the bell jar will come loose. As mentioned above, if you had the N2 tank on too high pressure, it will make a popping noise and jump up a bit. This is not good.
11. Toggle the vent off and turn off the N_2 upstream.
12. Raise the bell jar up as high as it will go on its cylindrical rail. This will be to its highest point (You have to lift it yourself, there are no motors) and then rotate it to right until it is over the crystal monitor. Lower the bell jar until it supports itself. It will stay in this state. It is out of the way from where you are working.
13. Put samples on to the rotation stage. Position the samples so that the evaporated atoms will have a straight shot at the surface when the shutter opens.

Preparing the evaporant-that is the material you will evaporate.

14. Replace the boats in the DENTON if they need replacing. Keep boats if you are using

the same material run to run. In some cases you will wish to empty out the old material.

14.1. Put the boat that requires the lowest current on the left since the transformer only supplies low voltage to it.

15. If it has been made opaque, replace the window glass (3" x 2" glass slide) so that you will have a place to see in to the evaporation area and will be able to see what is going on once the boats or filaments are hot.
16. Check that the XTAL crystal has life left. You do this by pushing the upper left number on the membrane control pad of the Inficon crystal thickness monitor. Right above it will be the words XTAL. It will give you the lifetime as percent used.
17. Check that the boot gasket is clean of dust by rubbing the bottom of it gently with a Kim wipe. Occasionally it will need to have a silicone grease applied. Do not do this until you are educated as to how it is done properly.
18. Carefully lower the bell jar, seeing that it seals all the way around.
19. Add LN_2 (liquid nitrogen) to the funnel and wait for it go into the trap.
20. You will do this periodically over next 10min. Stop when condensation starts to drip off of the outside of the funnel. The condensation is liquid air, not water.
21. Check the time. If more than 12-20 minutes has passed since step 6, the high vacuum pump will be pumping at optimum speed. If not, it will probably be ready when you have roughed out the system.

Roughing the system

22. Close the BACKING VALVE. (The diffusion pump is now not being actively "backed". This is okay if the time doesn't go over a minute or so).
23. Open the ROUGHING VALVE (toggle switch) and start T_{Rough}. Turn Pressure selector

gauge to chamber.

24. When the pressure drops below 100 mTorr stop T_{ROUGH} and record it in the logbook. This is usually less than about two minutes.
25. Close ROUGHING VALVE (toggle switch on the left) and then open the BACKING VALVE (toggle switch next to roughing).

Switching to High vacuum

26. Open the HI-VAC VALVE via the toggle switch, start $T_{High\ VAC}$.
27. Turn on the high vacuum gauge, record T_{HIGH} when the pressure reaches $1 * 10^{-5}$ Torr.
28. Wait until chamber drops below $3*10^{-6}$ Torr. This can take around 30 minutes. Add LN_2, if it takes longer. You can do the next step while you wait.

Doing the Evaporation

29. The Crystal Monitor should be on.
30. Use the Program button to switch to the desired material and check its parameters.
31. Set the final thickness desired and record these in the logbook. Zero the crystal by hitting the 3 button.
32. Turn on rotation.
33. Switch to the desired source. The choices are Left/ Right.
34. Turn on the Fil/Glow Power switch and ramp up the voltage with a rate of 10%/30seconds.
35. Current should never exceed 200 A, and voltage should remain below 80%.
36. The boat or coil will start to glow and get brighter as it evaporates.
37. Adjust the voltage to achieve desired rate of 20-100 Å /seconds—it depends on the material—then turn off the Fil/Glow Power switch when the voltage reaches 0%.

38. Do you need to do the other source? Repeat steps 27-35. Otherwise, go to the next line.

If you are done for the day, turn off the high vacuum pump.

39. You may turn off the High Vacuum GAUGE (this is not the same thing as the PUMP). The next step will also do this automatically, however.
40. Close High Vacuum Valve.
41. Open the N_2 tank and then the VENT VALVE.
42. Repeat steps 8-13 to open the bell jar.
43. If you are doing more coating today, go back to step 8.
44. If you are done for the day:
    - 44.1. Make sure that you have turned off the high vacuum pump.
    - 44.2. Lower the bell jar.
    - 44.3. Close the Backing Valve.
    - 44.4. Open the Roughing Valve.
    - 44.5. Bring down the system to 20 mTorr.
    - 44.6. Close all of the valves.
    - 44.7. Turn off the roughing pump and the high vacuum pump.
    - 44.8. Turn off the power.

References

[i] Özgür, U., Hofstetter, D., & Morkoç, H. (2010). *Proc. of the IEEE, 98*(7), 1255-1268. doi:10.1109/JPROC.2010.2044550

[ii] Fan, J. C., Sreekanth, K. M., Xie, Z., Chang, S. L., & Rao, K. V. (2013). *Progress in Materials Science, 58*(6), 874. doi: 10.1016/j.pmatsci.2013.03.002

[iii] Look, D. C., Claflin, B., Alivov, Y. I., & Park, S. J. (2004). The future of ZnO light emitters. *Physica Status Solidi (a), 201*(10), 2203-2212. doi:10.1002/pssa.200404803

[iv] Look, D., Burgener, R., Sizelove, J., & Renlund, G. (2004). As-doped p -type ZnO produced by an evaporation⁄sputtering process. *Applied Physics Letters, 85*(22), 5269-5271. doi:10.1063/1.1825615

[v] Bergener, R. et. al. (2006). *U.S. Patent No. US 7141489 B2*. Retrieved from https://patents.justia.com/patent/7141489

[vi] Peterson, Ryan. *Sputtering p-type Arsenic-doped Zinc Oxide Thin Films*, BYU Physics Department Senior Thesis (2018), https://www.physics.byu.edu/docs/thesis/794

[vii] J.A. Woollam Co. What is ellipsometry? Retrieved from https://www.jawoollam.com/resources/ellipsometry-tutorial/what-is-ellipsometry

[viii] Strein, Elisabeth. *Studying and Eliminating Adventitious Carbon Contamination on Silicon Wafers*, BYU Physics Department Senior Thesis (2008)

[ix] Crystal. (n.d.). In *Wikipedia*. Retrieved April 17, 2019, from https://en.wikipedia.org/wiki/Crystal

[x] Rivera, Felipe. *Electron Microscopy Characterization of Vanadium Dioxide Thin Films and Nanoparticles*, BYU Physics Department Ph.D. Dissertation, (2012), https://scholarsarchive.byu.edu/etd/2975

[xi] Shelley, Micah. *RF Magnetron Sputtering of Arsenic-doped p-type Zinc Oxide*, BYU Physics Department Senior Thesis (2019)